Journal of Molecular Graphics and Modelling 93 (2019) 107447

Contents lists available at ScienceDirect

Journal of Molecular Graphics and Modelling

journal homepage: www.elsevier.com/locate/JMGM

Evaluation of nonlinear optical properties from molecular descriptors of benzimidazole metal complexes by principal component analysis

P.A. Praveen [a, b], R. Ramesh Babu [b, *]

[a] Department of Physics, Indian Institute of Science Education and Research, Tirupati, 517 507, Andhra Pradesh, India
[b] Crystal Growth and Thin Film Laboratory, Department of Physics, Bharathidasan University, Tiruchirappalli, 620 024, Tamilnadu, India

ARTICLE INFO

Article history:
Received 18 July 2019
Received in revised form
30 August 2019
Accepted 30 August 2019
Available online 4 September 2019

Keywords:
Benzimidazole metal complexes
Transition metals
Semiempirical
PM6
Nonlinear optics

ABSTRACT

In the present work, semiempirical quantum chemical method (PM6) has been used for the simulation of molecular descriptors of first row transition metal ions incorporated benzimidazole metal complexes. Metal complexes with and without substituents are considered for the analysis. In both the cases, molecules show distinct properties with respect to the molecular descriptors. Since the dimension of the data set is large, principal component analysis has been used and the obtained principal components, PCA1 and PCA2, are linearly regressed with hyperpolarizability values. The obtained results indicate that molecular energy plays a dominant role in the nonlinear optical properties of benzimidazole metal complexes. Further, it is observed that the bond angle, global hardness and heat of formation of the molecules have considerable impact on the hyperpolarizability values.

1. Introduction

Nonlinear optics is one of the key fields to be explored for potential photonics applications [1–3]. Both inorganic and organic materials are widely investigated to suit the needs of nonlinear optics [4,5]. In which organic materials possess certain advantages such as molecular tailorability, high polarizability etc., however, they lack physical durability and lossless optical transmission. On the other hand, inorganic materials are stable, but it is not easy to modify their structure. So tailoring or improving the polarizability of inorganic materials is tedious. Hybrid materials like metal-organic complexes are proposed to utilize both the advantages of organic and inorganic materials [6,7]. In the recent past many such materials are reported in literature, in particular on the second and third order nonlinearity for optical bistability, frequency conversion and optical limiting applications. Benzimidazole metal complexes are one among those, which shows better physical and optical properties than their parent ligand. Our previous works on metal benzimidazole complexes (MBMZ) show that the nonlinear optical properties of the sample varies with respect to the type of metal ion and the substituents [8,9]. Further, the role of different molecular parameters in determining molecular polarizability and hyperpolarizability using semiempirical calculations are also reported [10]. But there is no systematic study available to evaluate the role of molecular parameters on structure-property relationships. In the present work, we have considered ten different molecular parameters, such as bond length, bond angle, energy gap, global hardness, molecular energy, heat of formation, dipole moment, intensity of vibrational frequency and linear polarizability to evaluate the first and second hyperpolarizability of first row transition metal complexes of benzimidazole. For the study, two types of metal complexes were considered, one without any substituent (Goodman Type (GMT)) [11] and the another one with chloride substituents [12]. The molecular parameters were extracted from the semiempirical quantum chemical calculations. In order to correlate the parameters, principal component analysis (PCA) was performed. The obtained first and second principal components from PCA was then linearly correlated with hyperpolarizability values.

2. Materials and methods

2.1. Structural description

Mostly, in MBMZ complexes, the metal-ligand bond occurred between N2 of the imidazole ring (Fig. 1) and the metal ion [12,13]. During the synthesis of MBMZ, in some cases, substituents like

* Corresponding author.
E-mail address: rameshbabu.r@bdu.ac.in (R.R. Babu).

https://doi.org/10.1016/j.jmgm.2019.107447
1093-3263/

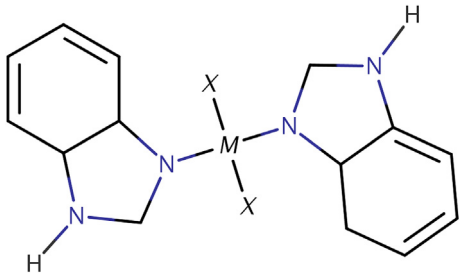

Fig. 1. Molecular structure of metal benzimidazole complex, where, M(= Sc, Ti, V, Cr, Mn, Fe, Co, Ni and Cu) is the metal ion and X(=Cl) is the substituent.

chlorides, iodides, bromides and acetates can also present in the complex. Often the inclusion of substituents has a positive impact on the nonlinear optical properties of molecules. Due to their low heat of formation values, it is easy to synthesize the Cl based complexes [10]. Considering this fact and comparing with the available reports, we reduce the problem to solve only for Cl based complexes. Fig. 1 shows the molecular structure of metal benzimidazole complex, where, M (Sc, Ti, V, Cr, Mn, Fe, Co, Ni and Cu) is the metal ion and X (Cl) is the substituent.

2.2. Computational methods

Semiempirical quantum chemistry program MOPAC2016 was used for all the calculations [14]. PM6 algorithm available in the package was used for the geometry optimization. A normalization value, GNORM = 1 was used for the system energy reduction and the optimized geometries were subjected to vibrational analysis to ensure that no negative frequencies was observed in the vibrational spectrum of the optimized system, which confirms the stability of molecular structure. If there is any discrepancy in the optimized geometry or in the vibrational spectrum, corresponding molecular structures were subjected to intermediate reaction coordinate (IRC) analysis to obtain a stable structure and then they were re-optimized. Static polarizability and hyperpolarizability values of the optimized geometries were calculated using TDHF formalism. Further, the auxiliary and output files derived from self-consistent field (SCF) calculation was used to calculate the dipole moment, HOMO, LUMO, energy gap (E_g), heat of formation and energy of the molecule. Gabedit package was used to visualize the HOMO and LUMO levels [15].

3. Results and discussion

3.1. Optimized geometry

Table 1 shows the optimized geometrical parameters of MBMZ complexes with and without chloride ion substituents. Considering dihedral angles, without Cl substituent, the angles increases from 134.3° to 179.2°, i.e., molecules show an increment trend from Ti to Mn. Whereas, for Fe, it decreases to 156.9°, then increases for Co. But once again it decreases for Ni and then increases for Cu. In case of Cl substituted complexes a down trend is observed for V and Cr, Co and Ni. This variation can be interpreted as due to the variation of electronic distribution caused by the incorporation of metal ions and the substitution of Cl ions. Further, the results indicates that the planarity of the molecules decreases with increase in the atomic number of the metal ions. Considering bond length, it decreases with increase in the atomic number of metal ions. But it shows an increment for Co and Ni complexes and decreases slightly for Cu complexes. On the other hand, Cl substituted complexes show decrement utpto Cr and then increases for Mn and Co complexes. The variation in the bond lengths can be attributed to the conjugation effect, which tends to produce a maximum overlap of lone pairs with the p_z orbitals [16,17].

Table 1
Calculated bond lengths (N-M) and bond angles (N-M-N) of first row transition metals incorporated BMZ complexes with and without Cl substituents.

	(N-M) (Å)		(N-M-N)(°)	
Molecule	GMT	Cl-MBMZ	GMT	Cl-MBMZ
Ti-BMZ	2.03	2.05	134.3	106.9
V-BMZ	1.92	1.90	138.0	104.0
Cr-BMZ	1.89	1.80	157.3	95.5
Mn-BMZ	1.79	1.83	179.2	149.3
Fe-BMZ	1.72	1.82	156.9	153.9
Co-BMZ	1.75	1.88	179.1	151.0
Ni-BMZ	1.89	1.83	177.0	112.8
Cu-BMZ	1.76	1.82	179.4	177.2

3.2. Electronic properties

Fig. 2 shows the calculated HOMO and LUMO orbitals of benzimidazole metal complexes with and without substituents. In the case of complexes without substituents, the HOMO is distributed over one ring in Fig. 2((I A) a-h), in Fig. 2((I A) a-d) it is located at the spot of metal ion. In other compounds, distribution over one ring trend is observed with more distribution range. Fig. 2((II A) a to e) is also shows the similar phenomenon discussed above. In the case of Fig. 2((II A) f to h), HOMO is distributed over the entire molecule. Considering LUMO, one ring distribution is observed for Fig. 2((I B) a-e) and other complexes such as in Fig. 2((I B) f-h) shows the complete LUMO distribution over the molecule. This indicates that the active sites are often distributed to one of the imidazolate ring and charge transfer between the molecule taken place through the metal ion. A similar phenomena is observed in the case of Cl substituted MBMZ complexes too (Fig. 2((II B) a-h)).

Further, from HOMO, LUMO and energy gap (E_g = LUMO-HOMO) the global hardness factor (η) was calculated using the relation $\eta = E_g/2$ [18]. This factor can be taken as a estimation of chemical hardness of a molecule and can be used to describe the reactive behaviour of the molecular system. From Table 2, the energy gap values of the metal complexes without substituents shows decreasing trend in the case of Cr and Co molecules and, Co complexes shows the lowest energy gap value in this series. In the case of Cl substituted complexes, V, Cr, Fe and Co shows the decrement trend and Co shows the lowest energy gap value. The reactivity order of benzimidazole metal complexes without substituents can be given as Mn < Cr < Ni < V < Ti < Cu < Fe < Co and for the complexes with substituents can be given as Co < Cr < V < Ni < Cu < Fe < Mn < Ti. It can be seen that the reactivity values decreases for the Cl substituted metal complexes, which indicates that these complexes are more stabilized than the complexes without substitution.

3.3. N-M stretching intensities

Stretching intensity of the imidazole nitrogen and metal ion (N-M) was calculated for MBMZ molecules, with and without substituents, from the vibrational analysis and is given in Table 3. It can be seen that there is a variation in frequency (ν) up to 50 cm^{-1} in both the cases depending on the type of metal ion and substituent. Further, there is a sharp variation in intensities ranging from 1000 to 12000 (Km/mol). Strong infrared intensities in the case of Ti, V and Co can be attributed to the back-donation of electrons from N1 of the imidazolate ring. But the saturation of d-levels in metal ions

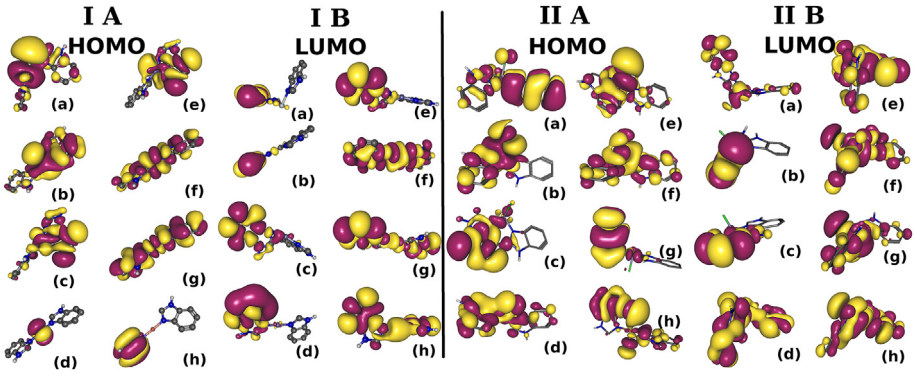

Fig. 2. HOMO and LUMO orbitals of benzimidazole metal complexes (IA & IB) without and (II A & II B) with Cl substituents: (a) Ti-BMZ (b) V-BMZ (c) Cr-BMZ (d) Mn-BMZ (e) Fe-BMZ (f) Co-BMZ (g) Ni-BMZ (h) Cu-BMZ, respectively.

Table 2
Calculated HOMO, LUMO, Band gap (E_g) and global hardness (η) of first row transition metals incorporated BMZ complexes with and without Cl substituents.

	HOMO (eV)		LUMO (eV)		E_g (eV)		η (eV)	
Molecule	GMT	Cl-MBMZ	GMT	Cl-MBMZ	GMT	Cl-MBMZ	GMT	Cl-MBMZ
Ti-BMZ	−0.2942	−0.3619	−0.0887	−0.0791	0.2055	0.2828	0.1914	0.1414
V-BMZ	−0.3048	−0.2863	−0.0688	−0.0588	0.2336	0.2275	0.1868	0.1137
Cr-BMZ	−0.2839	−0.3074	−0.0837	−0.0847	0.2002	0.2227	0.1838	0.1113
Mn-BMZ	−0.2817	−0.3173	−0.0767	−0.0508	0.2054	0.2665	0.1792	0.1332
Fe-BMZ	−0.3134	−0.3128	−0.0944	−0.0636	0.2197	0.2492	0.2039	0.1246
Co-BMZ	−0.2953	−0.2416	−0.1373	−0.1285	0.1581	0.1131	0.2163	0.0565
Ni-BMZ	−0.3161	−0.3388	−0.0564	−0.1032	0.2597	0.2356	0.1862	0.1178
Cu-BMZ	−0.3500	−0.3398	−0.0400	−0.0976	0.3142	0.2422	0.1950	0.1211

Table 3
N-M stretching intensities of first row transition metals incorporated BMZ complexes with and without Cl substituents.

	GMT		Cl-MBMZ	
Molecule	ν cm^{-1}	Intensity (Km/mol)	ν cm^{-1}	Intensity (Km/mol)
Ti-BMZ	399	11871	397	11947
V-BMZ	398	11492	357	16036
Cr-BMZ	354	2906	405	1872
Mn-BMZ	406	1286	334	9160
Fe-BMZ	390	1148	417	2601
Co-BMZ	375	8136	358	7847
Ni-BMZ	429	5089	424	3298
Cu-BMZ	384	3844	400	1544

greatly affects the back-donation and in the case of Cl substituents sharing of electron density play a significant role in the vibrational intensities. Drastic shift observed in the case of Cr and Ni without substituents, and V, Mn and Co with substituents can be attributed to the Fermi resonance due to the deformation of imidazolate ring [19,20]. Since it is not a common phenomena, more analytical work is required to deduce the high unharmonic coupling in molecular deformation to explain such a drastic variation in frequency.

3.4. Molecular energy and point group

Table 4 shows molecular energy (E), heat of formation (HOF), molecular dipole moment (μ) and point groups of benzimidazole metal complexes with and without substituents. Except Co complex (in both the cases), for all other complexes, the molecular energy increases with increase in atomic number. Degenerated d-shells could be the reason for such a variation in the case of Co complex. HOF values of the complexes without substituent shows an increment trend with respect to atomic numbers for the case of Ti, V and Cr, but decreases for Mn, Fe and Co complexes. In the case of Cl substituted complexes decrement is observed for Cr complex alone and for all other MBMZ complexes an increment trend has been observed. Further analysis is required to explain this phenomena. The point groups are generated based on the molecular deformation due to metal ions and substituents. From our results, it can be seen that there is no strict relation between the molecular point group and molecular energy/HOF values of MBMZ.

3.5. Polarizability and hyperpolarizability analysis

Table 5 shows the calculated static polarizability and hyperpolarizability values of MBMZ complexes with and without substituents. Considering linear polarizability, molecules without substituents have the values between 2 and 8.72 ($\times 10^2$) atomic units, and Cr complex shows the highest polarizability. Cl substitution induces a positive impact on linear polarizability and it increases to many folds in the case of V, Cr and Fe. Complexes without substituents shows β values between 1.36 and 8.74 ($\times 10^3$ a.u.) and V and Co have the higher values about 8.74 and 8.30 ($\times 10^3$ a.u.) respectively. Further, Cl substituents improves the first order hyperpolarizability values by many folds, particularly Co and Ni shows β values higher than 100×10^3 a.u. The γ values of benzimidazole metal complexes are between 1.17 and 8.18 $\times 10^5$ a.u., in which, Cr and Fe shows the high γ values. Cl substituted MBMZ complexes have a positive impact on the second order hyperpolarizability, in particular Mn complex shows the highest γ value.

3.6. Correlation between molecular descriptors

From the results discussed above, it is not possible to derive a conclusion on the effect of different parameters on nonlinear optical properties due to the higher dimensionality of data set.

Table 4
Calculated molecular energy (E), heat of formation (HOF), molecular dipole moment (μ) and point groups of first row transition metals incorporated BMZ complexes with and without Cl substituents.

	E (eV)		HOF (kcal/mol)		μ (debye)		Point group	
Molecule	GMT	Cl-MBMZ	GMT	Cl-MBMZ	GMT	Cl-MBMZ	GMT	Cl-MBMZ
Ti-BMZ	−2509	−3022	495.15	394.56	3.95	3.48	C_1	C_1
V-BMZ	−2546	−3057	526.58	454.04	3.57	3.42	C_1	C_1
Cr-BMZ	−2627	−3143	586.13	414.60	7.30	7.59	C_1	C_s
Mn-BMZ	−2638	−3149	545.09	471.81	0.39	3.49	C_2	C_1
Fe-BMZ	−2870	−3381	534.87	475.60	6.41	1.87	C_1	C_1
Co-BMZ	−2612	−3121	529.66	509.92	1.31	5.93	C_2h	C_1
Ni-BMZ	−2927	−3437	568.83	544.27	0.20	4.91	C_2	C_1
Cu-BMZ	−3097	−3607	592.87	547.60	0.94	5.10	C_1	C_1

Table 5
Calculated static polarizability and hyperpolarizability values of first row transition metals incorporated BMZ complexes with and without Cl substituents.

	$\alpha \times (10^2)$ (a.u.)		$\beta \times (10^3)$ (a.u.)		$\gamma \times (10^5)$ (a.u.)	
Molecule	GMT	Cl-MBMZ	GMT	Cl-MBMZ	GMT	Cl-MBMZ
Ti-BMZ	2.09	18.45	2.51	30.14	6.37	11.28
V-BMZ	3.96	60.94	8.74	57.83	4.09	74.57
Cr-BMZ	8.72	29.05	1.36	2.60	8.08	5.72
Mn-BMZ	2.00	8.57	1.46	13.42	5.39	97.47
Fe-BMZ	3.40	27.45	6.23	65.21	8.18	78.18
Co-BMZ	2.83	3.66	8.30	149.95	1.17	48.06
Ni-BMZ	2.10	5.73	4.78	102.51	3.53	13.05
Cu-BMZ	2.62	2.74	4.99	9.20	3.21	14.93

Principal component analysis (PCA) is one of the potential methods used to reduce higher-dimensionality of the data sets and the details of the analysis is described elsewhere [21]. In the present study, simulated semiempirical parameters were subjected to statistical analysis, performed using R package (http://www.r-project.org). Loadings and scores matrices are the two main outputs from the PCA analysis. In which, loading plot is used to identify the important variables, whereas, scores are used to describe the spatial distribution of samples on new axes called as principal components (PC). PC are considered as the dependent variable for regression and analysis of variance. Interpretation of PC is based on the fact that the most strongly correlated components are the one, farthest from the zero point either in positive or negative direction.

3.7. Scores, loadings and biplots

Fig. 3 shows the projection of the original variables in the same space (loading plot), it can be seen that the substituents (X), molecular energy (E) and dipole moment (MU) show- positive values and the bond length (BL), intensity of vibrational frequency (INT) and linear polarizability (ALP) show the negative values, corresponding to a positive and negative phenomenon in the PC1 and PC2 respectively. Fig. 4 shows the projection of the simulated molecular descriptors defined by two principal components (score plot) [22].

In order to visualize and interpret loadings and scores together, biplot is a very useful tool. In which two variables, which are close and far from the origin, are correlated with respect to the variation in molecular components [23]. Fig. 5 shows the correlation biplot of PC1 and PC2. The center of the plot implies the average sample (not zero) and the points with low values are relative to other samples and the points with higher values are more independent.

3.8. Scree test

Scree test is used to validate the PCA calculations [21]. The test graph is plotted as the function of number of components and when only noise is modeled, the eigen values are decline gradually. In practice, due to the large eigen values, it is difficult to visualize the results and in such a case logarithmic values are plotted and shown in Figs. 6 and 7. The gradual decrement with respect to the principal component ensures the validation of study.

3.9. Analysis

3.9.1. First principal component - PCA1

The first principal component (PCA1) can be interpreted as a quantitative variable, that provides the overall predictive ability of the different sets of molecular descriptors for all the selected properties, the loadings of all the original variables (molecular properties) being positive in this component. From Fig. 3, it can be seen that the first principal component increases with increasing molecular energy (E) and linear polarizability (ALP) and decreases with bond angle (BA), global hardness value (ETA) and heat of

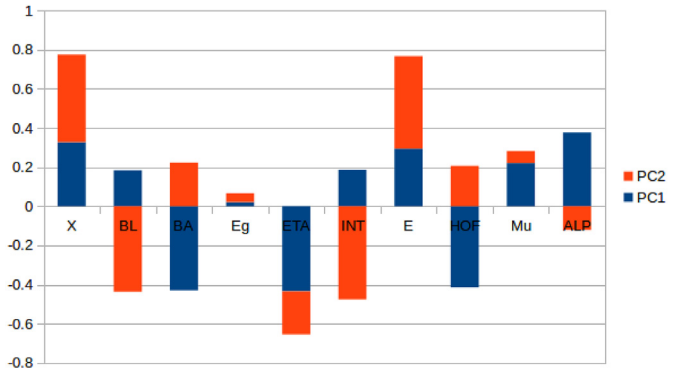

Fig. 3. Loadings plot of PCA1 and PCA2.

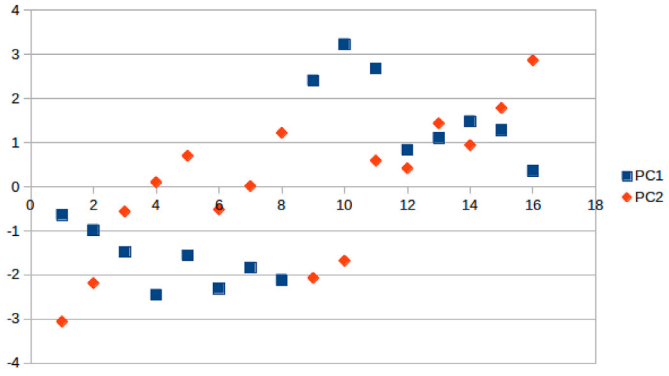

Fig. 4. Scorings plot of PCA1 and PCA2.

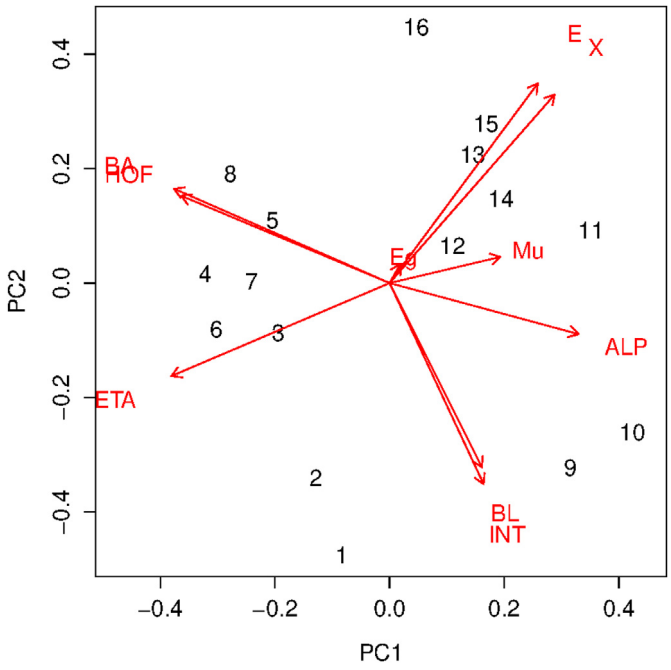

Fig. 5. Correlation biplot of PCA1 and PCA2.

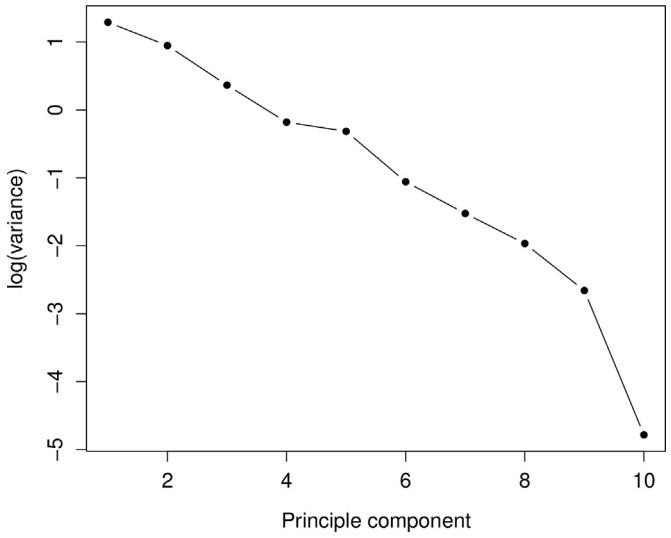

Fig. 6. Scree plot of PCA1 and PCA2.

formation (HOF) scores. This suggests that these five criteria vary together. If BA, ETA and HOF decreases correspondingly E and ALP increases. In other words, the first principal component can be used to distinguish between sets of molecular descriptors that, in general, perform well with all the considered properties (to the right in the score plot of Fig. 3) and those with low overall prediction power (to the left in the score plot). Therefore, it can be concluded that the best models are mixed models, based on descriptors.

3.9.2. Second principal component - PCA2

The second principal component increases with decrease in BL and INT values and with increase in molecular energy. This indicates the increase in molecular energy with respect to bond length and correspondingly to the vibrational intensity. The

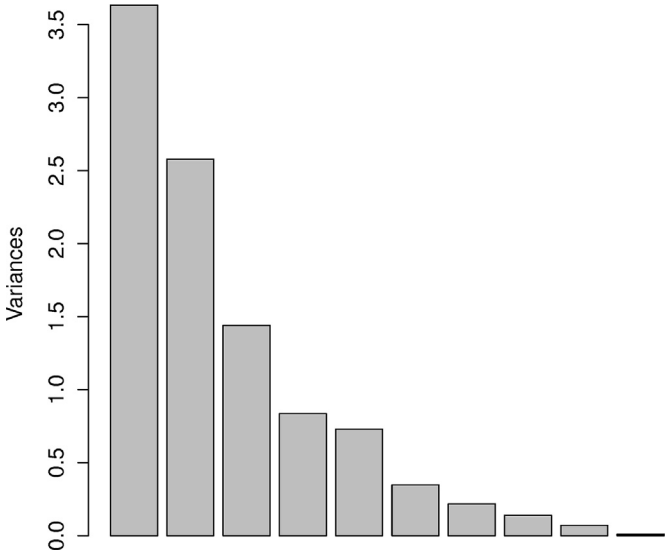

Fig. 7. Logarithmic Scree plot of PCA1 and PCA2.

analysis can be completed by interpreting scatter plot of scores. In which each dot represents a member of a cluster and the lower and higher PCA1 values shows that the particular member has high influence (positive and negative, respect to the high and low values) on molecular properties. An reverse effect is expected from PCA2, i.e., positive for lower and negative for higher values.

3.9.3. PCAs Vs hyperpolarizability

In order to correlate the principal components 1 and 2, the three dimensional data as two dimensional plots (Figs. 8 and 9) were drawn. In which, the variation of hyperpolarizabilities with respect to principal components is shown and the hyperpolarizabilities are designated in a colour scale ranging from dark blue (zero) to pale yellow (160). Here the idea is to discuss the influence of principal components on nonlinear optical properties rather than to discuss which one provides better hyperpolarizabilities. Because, the influence of principal components can be interpreted in either way, i.e., they may contribute either positively or negatively. So, whether the hyperpolarizabilities are high or low, more the principal component value, higher its influence on the particular property in a particular complex. From Fig. 8 except non-Cl substituted Ti and V, in all other cases PCA2 dominates over PCA1. Certainly, there is an equal effect observed from Cl substituted Co, but the trend is mainly dominates by PCA2. In second order hyperpolarizability studies combined effect of PCA1 and PCA2 is observed (Fig. 9) for Cl substituted Mn, Fe and Co. But for Cl substituted Ti, V and Cr, PCA1 dominates and for Ni and Cu, PCA2 dominates. Overall, dominant effect of PCA2 have been observed for MBMZ complexes.

4. Conclusion

Different molecular descriptors were calculated using the semiempirical quantum chemical calculations. They were correlated by means of principal component analysis and the first principal component shows strong correlation between molecular energy and linear polarizability and decreases with bond angle, global hardness value and heat of formation scores. In the case of second principal component BL and INT decreases and the molecular energy increases. These components provide a strong base to evaluate the nonlinear optical properties of the first row transition metal complexes.

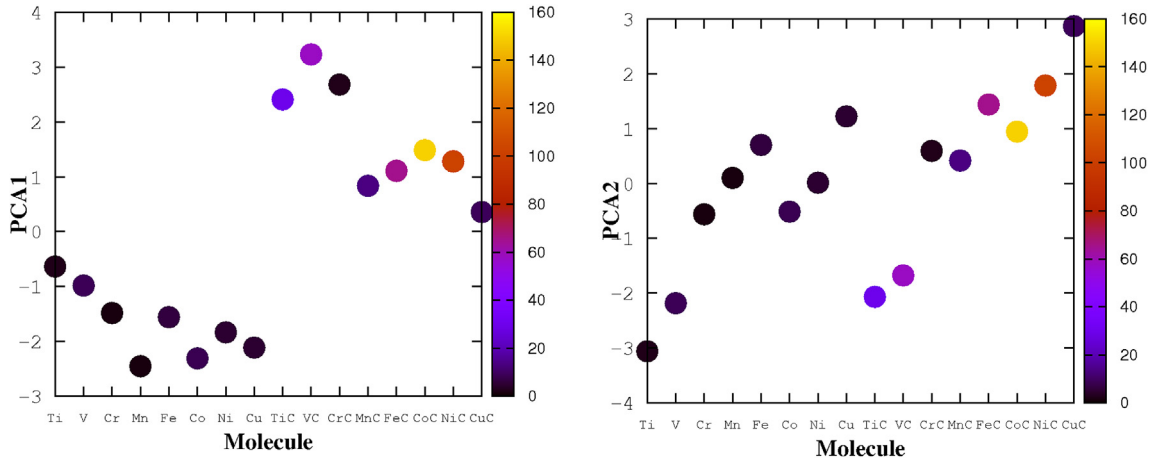

Fig. 8. Linear regression of first hyperpolarizability with (a) PCA1 and (b) PCA2 for MBMZ complexes with and without Cl substituents.

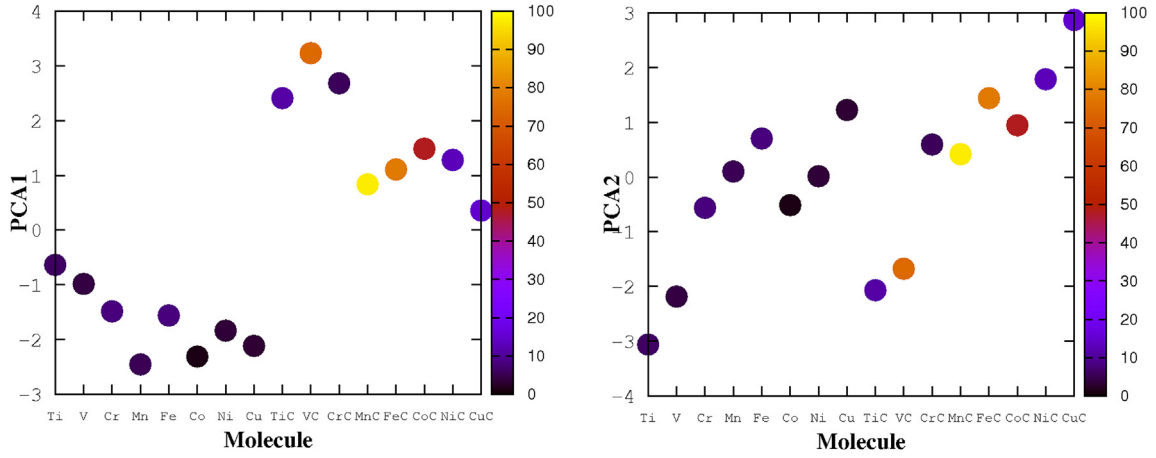

Fig. 9. Linear regression of second hyperpolarizability with (a) PCA1 and (b) PCA2 for MBMZ complexes with and without Cl substituents.

Acknowledgments

Authors acknowledge the financial assistance from School of Physics, provided by DST-FIST (Order No: SR/FIST/PSI-204/2015 (c)) for the establishment of research facilities. Further, one of the authors P.A. Praveen thank the UGC-BSR, Govt. of India for financial assistance in the form of 'Research Fellowship in Science for Meritorious Students' (F.4-1/2006/7-197/2007(BSR)). Also he thank Dr. T. Kanagasekaran, Department of Physics, IISER Tirupati for fruitful discussions.

References

[1] J. Zyss, Molecular Nonlinear Optics: Materials, Physics, and Devices, Academic press, 2013.
[2] X. Yin, Z. Ye, D.A. Chenet, Y. Ye, K. O'Brien, J.C. Hone, X. Zhang, Edge nonlinear optics on a MoS_2 atomic monolayer, Science 344 (2014) 488–490.
[3] D.E. Chang, V. Vuletić, M.D. Lukin, Quantum nonlinear optics photon by photon, Nat. Photonics 8 (2014) 685–694.
[4] X. Liu, Q. Guo, J. Qiu, Emerging low-dimensional materials for nonlinear optics and ultrafast photonics, Adv. Mater. 29 (2017), 1605886.
[5] P.G. Lacroix, I. Malfant, C. Lepetit, Second-order nonlinear optics in coordination chemistry: an open door towards multi-functional materials and molecular switches, Coord. Chem. Rev. 308 (2016) 381–394.
[6] B.S. Kalanoor, L. Gouda, R. Gottesman, S. Tirosh, E. Haltzi, A. Zaban, Y.R. Tischler, Third-order optical nonlinearities in organometallic methylammonium lead iodide perovskite thin films, ACS Photonics 3 (2016) 361–370.
[7] D. Dini, M.J. Calvete, M. Hanack, Nonlinear optical materials for the smart filtering of optical radiation, Chem. Rev. 116 (2016) 13043–13233.
[8] P.A. Praveen, R. Ramesh Babu, K. Jothivenkatachalam, K. Ramamurthi, Spectral, morphological, linear and nonlinear optical properties of nanostructured benzimidazole metal complex thin films, Spectrochim. Acta A Mol. Biomol. Spectrosc. 150 (2015) 280–289.
[9] P.A. Praveen, R. Ramesh Babu, K. Ramamurthi, Role of annealing on the structural and optical properties of nanostructured diaceto bis-benzimidazole Mn (II) complex thin films, Spectrochim. Acta A Mol. Biomol. Spectrosc. 173 (2017) 800–808.
[10] P.A. Praveen, R. Ramesh Babu, Effect of substituents on polarizability and hyperpolarizability values of benzimidazole metal complexes, AIP. Conf. Proc. 1731 (2016), 090013(1-3).
[11] T.J. Lane, K.P. Quinlan, Metal binding of the benzimidazoles, J. Am. Chem. Soc. 82 (1960) 2994–2997.
[12] E. Sahin, S. Ide, M. Kurt, S. Yurdakul, Structural investigation of dibromobis (benzimidazole) Zn (II) complex, J. Mol. Struct. 616 (2002) 259–264.
[13] S. Yurdakul, M. Kurt, Vibrational spectroscopic studies of metal (II) halide benzimidazole, J. Mol. Struct. 650 (2003) 181–190.
[14] P.O. Dral, X. Wu, L. Sporkel, A. Koslowski, W. Thiel, Semiempirical quantum-chemical orthogonalization-corrected methods: benchmarks for ground-state properties, J. Chem. Theory Comput. 12 (2016) 1097–1120.
[15] A.-R. Allouche, Gabedit—a graphical user interface for computational chemistry softwares, J. Comput. Chem. 32 (2011) 174–182.
[16] H.A. Bent, An appraisal of valence-bond structures and hybridization in compounds of the first-row elements, Chem. Rev. 61 (1961) 275–311.
[17] J.-L. Brédas, Relationship between band gap and bond length alternation in organic conjugated polymers, J. Chem. Phys. 82 (1985) 3808–3811.
[18] L.M. Rodriguez-Valdez, A. Martínez-Villafañe, D. Glossman-Mitnik, Computational simulation of the molecular structure and properties of heterocyclic organic compounds with possible corrosion inhibition properties, J. Mol. Struct.: THEOCHEM 713 (2005) 65–70.

[19] M. Rumi, G. Zerbi, Conformational dependence of vibrational and molecular nonlinear optical properties in substituted benzenes: the role of π-electron conjugation and back-donation, J. Mol. Struct. 509 (1999) 11–28.
[20] S. Choi, T.G. Spiro, Out-of-plane deformation modes in the resonance Raman spectra of metalloporphyrins and heme proteins, J. Am. Chem. Soc. 105 (1983) 3683–3692.
[21] R. Bro, A.K. Smilde, Principal component analysis, Anal. Methods 6 (2014) 2812–2831.
[22] I. Algül, D. Kara, Determination and chemometric evaluation of total aflatoxin, aflatoxin B1, ochratoxin A and heavy metals content in corn flours from Turkey, Food Chem. 157 (2014) 70–76.
[23] C. Chapman, E.M. Feit, R for Marketing Research and Analytics, Springer, 2015, pp. 195–223.